Analysis & Sensing

Chemistry Europe
European Chemical Societies Publishing

Cover Feature:
K. E. Borbas and co-workers
Analysis of Anion Binding Effects on the Sensitized Luminescence of Macrocyclic Europium(III) Complexes

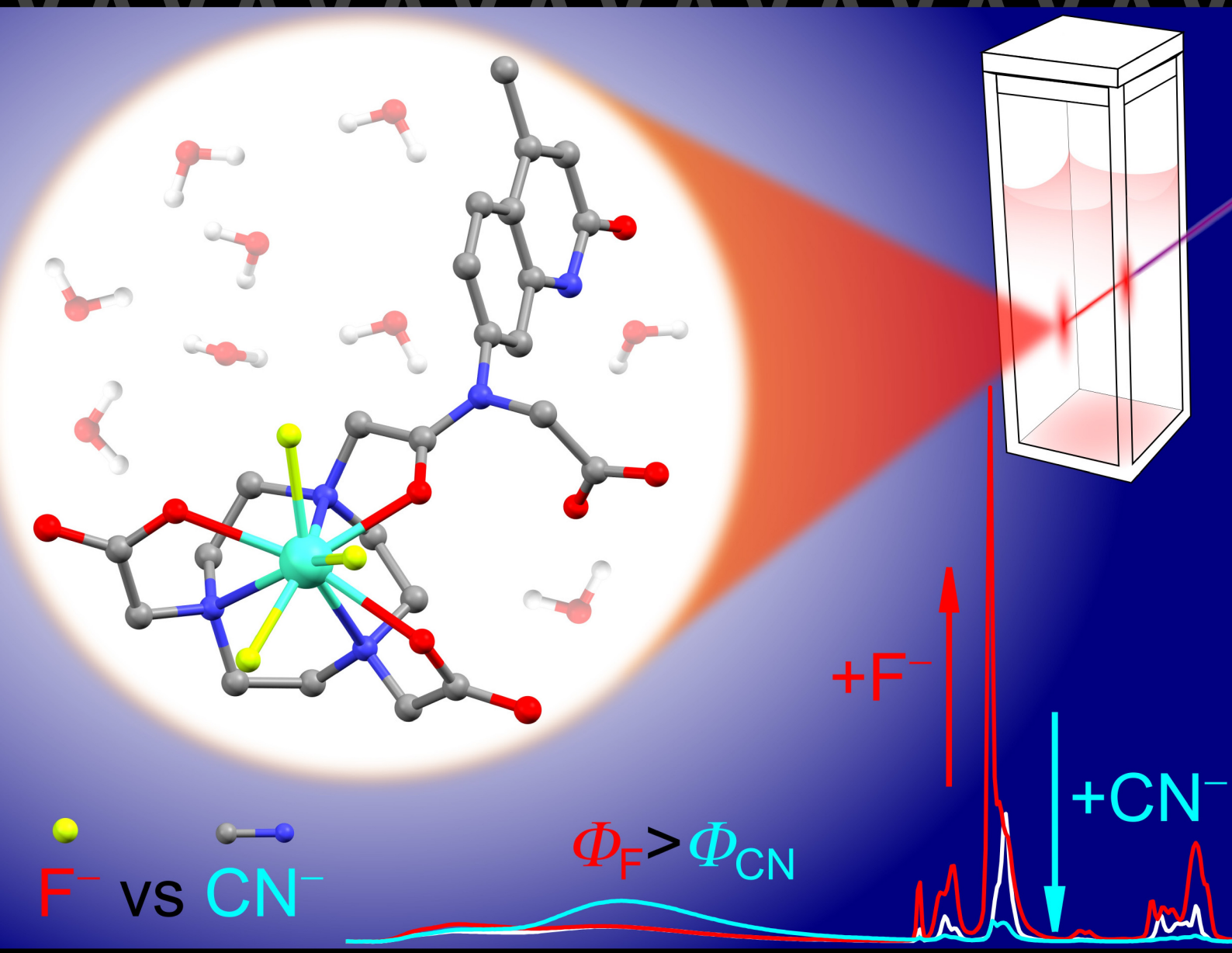

WILEY-VCH
6/2022

Analysis & Sensing

Research Article
doi.org/10.1002/anse.202200015

Chemistry Europe
European Chemical Societies Publishing

www.analysis-sensing.org

Special Collection

Analysis of Anion Binding Effects on the Sensitized Luminescence of Macrocyclic Europium(III) Complexes

Salauat R. Kiraev,[a] Roza R. Weber,[a] Jordann A. L. Wells,[a] Andreas Orthaber,[a] Daniel Kovacs,[a] and K. Eszter Borbas*[a]

Four triazamacrocyclic and two tetraazamacrocyclic ligands carrying two and three coordinating donor groups, respectively, and a carbostyril light-harvesting antenna were synthesized. The antenna was linked to a macrocycle either via secondary or tertiary amide. Complexation with europium (Eu), gadolinium (Gd), terbium (Tb), and ytterbium (Yb) yielded overall +1 or +2 charged species. Paramagnetic ^{1}H NMR, and steady-state and time-resolved luminescence spectroscopies showed that the complexes had 1–3 inner-sphere water molecules and displayed a variety of coordination geometries in solution. The antennae sensitized Eu(III) and Tb(III) emission with quantum yields of 0.3–4.3% and 9.9–24.5%, respectively. The addition of excess fluoride or cyanide to buffered Eu(III) complex solutions resulted in anion-dependent changes. Fluoride addition increased the Eu(III) luminescence intensity by displacing all inner-sphere water molecules and stabilizing the +3 oxidation state of Eu. Eu(III) luminescence increased up to 25-fold for one emitter. Cyanide quenched Eu(III) luminescence in all cases despite partial water ligand displacement.

Introduction

The luminescent properties of trivalent lanthanide (Ln(III)) coordination compounds are in many ways superior to those of more established organic fluorophores. The emission spectra consist of sharp signals, which in the case of Eu(III) and Tb(III) have ms range lifetimes.[1] The positions of the Ln(III) electronic transitions are less affected by the ligand environment than that of *d*-metal ions, and thus can serve as readily recognizable fingerprints.[2] For these reasons Ln(III) emitters are well suited for detection in complex environments, such as sensing in biological systems[3] and in industrial settings.[4]

Ln(III) luminescence arises from Laporte-forbidden f-f transitions, and is commonly sensitized via light-harvesting antennae.[1] The overall Ln(III) luminescence quantum yield (Φ_{Ln}) is the product of the population efficiency of the Ln(III) excited state (sensitization efficiency, η_{sens}) and the ability of the excited Ln(III) to emit light (intrinsic quantum yield, Φ_{Ln}^{Ln}, Eq. 1).[5]

$$\Phi_{Ln} = \eta_{sens} \cdot \Phi_{Ln}^{Ln} \quad (1)$$

Analyte detection may rely on the analyte's ability to modulate either η_{sens} or Φ_{Ln}^{Ln}, or both, although the origins of the change are often unclear. We have recently found that the emission intensity of a +3 charged Eu(III) complex increased 7.6-fold upon fluoride binding.[6] Fluoride replaced a Eu-bound water molecule, and the emission intensity increase was due to two factors. First, the removal of quenching inner-sphere O–H oscillators increased Φ_{Ln}^{Ln} 2.29-fold. Second, η_{sens} increased 3.35-fold because photoinduced electron transfer (PeT) from the excited antenna to Eu(III) is diminished in the fluoride-containing complex compared to that of the water-bound one. As PeT is a quenching process in most Eu(III) emitters,[7] its suppression results in an improved η_{sens}, and thus an increased Φ_{Ln} (Figure 1). The fact that even minor structural changes can affect PeT was made clear when fluoride was added to a Eu(III) complex with the same macrocycle and antenna, but a tertiary rather than a secondary amide linker. In the latter case, fluoride addition increased Φ_{Ln} 4.4-fold due to 2.1-fold increases in both Φ_{Ln}^{Ln} and η_{sens}.[8] We hypothesized that the contributions of fluoride binding to changes in Φ_{Ln}^{Ln} and η_{sens} are dependent on the complex and ligand structures, the antenna orientation, as well as the presence of other competing quenching processes. A detailed exploration of the origins of emission change would therefore enable the optimization of the luminescence response.

Here, we evaluate the effects of fluoride and cyanide binding to a variety of Eu(III) emitters based on macrocyclic ligands (Figure 2). The complex binding sites have overall positive charges ranging from +1 to +3 and at least a single Ln(III)-bound water molecule. Ligands are based on 1,4,7-triazacyclononane- (TACN, **Lt**) or 1,4,7,10-tetraazacyclododecane (cyclen, **Lc**), and are functionalized with methylenecarboxylate, methylenecarbamide, or picolinate (**Lp**) donors to complete the ligand sphere. All complexes were

[a] S. R. Kiraev, R. R. Weber, Dr. J. A. L. Wells, Dr. A. Orthaber, Dr. D. Kovacs, Prof. K. E. Borbas
Department of Chemistry, Ångström Laboratory
Uppsala University
Box 523, 75120 Uppsala (Sweden)
E-mail: eszter.borbas@kemi.uu.se

Supporting information for this article is available on the WWW under https://doi.org/10.1002/anse.202200015

Special Collection *Part of a Special Collection focusing on luminescence sensing.*

© 2022 The Authors. Analysis & Sensing published by Wiley-VCH GmbH. This is an open access article under the terms of the Creative Commons Attribution Non-Commercial License, which permits use, distribution and reproduction in any medium, provided the original work is properly cited and is not used for commercial purposes.

© 2022 The Authors. Analysis & Sensing published by Wiley-VCH GmbH.

Research Article
doi.org/10.1002/anse.202200015

Chemistry Europe
European Chemical Societies Publishing

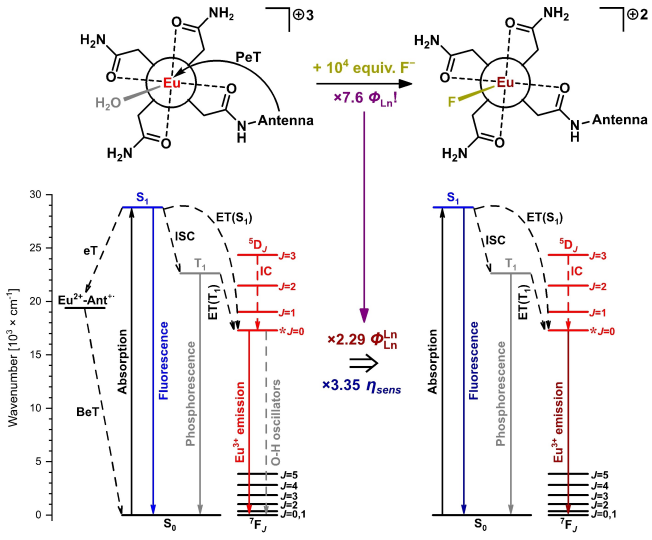

Figure 1. Jablonskii diagram for Eu(III) complex illustrating the effect of fluoride binding on Eu(III) luminescence and the consequences of altered sensitization efficiency and intrinsic quantum yield.[6] ISC = intersystem crossing, IC = internal conversion, ET = energy transfer, (B)eT = (back) electron transfer, solid and dashed arrows indicate radiative and nonradiative processes, respectively.

appended with 4-methyl- (Me) or 4-methoxymethyl-7-aminocarbostyril (MOM) antennae. We expected that the variety of ligand environments would allow for diverse combinations of Φ_{Ln}^{Ln} and η_{sens} which would in turn be affected to varying degrees by anion binding. Our hypothesis was that the target anions would replace inner-sphere water ligands, as has been shown for a number of fluoride probes,[9] and one cyanide probe.[10] A turn-on response for these probes can be explained by the removal of quenching O–H oscillators. However, models of anion detection that take only the removal of the water ligand into account make the differentiation between anions with similar steric demands, coordination modes, and charges (e.g. fluoride or cyanide) difficult. By taking into consideration the influence that anion binding has on the Ln(III), even similar anions may be differentiated based on their unique combination of effects on Φ_{Ln}^{Ln} and η_{sens}. Our results show that cyanide and fluoride are sufficiently different to be distinguished based on their electronic properties, which are rarely considered in Ln(III)-based probes. Furthermore, evaluating Φ_{Ln}^{Ln} and η_{sens} changes in complexes upon fluoride addition provides an understanding of the factors that contribute to a turn-on response upon water replacement, and the structural features that maximize these (i.e. which increase Φ_{Ln}^{Ln} and which ones improve η_{sens}).

Results and Discussion

Complex design

The metal binding sites have overall positive charges which in some cases are partially balanced by the presence of a non-coordinating methylcarboxylate substituent in the linking amide, and chloride counterions. Antennae are based on easily prepared 4-substituted 7-aminocarbostyrils (2-quinolones) which can efficiently sensitize not only Eu(III) and Tb(III), but also Sm(III), Dy(III), Nd(III) and Yb(III).[11]

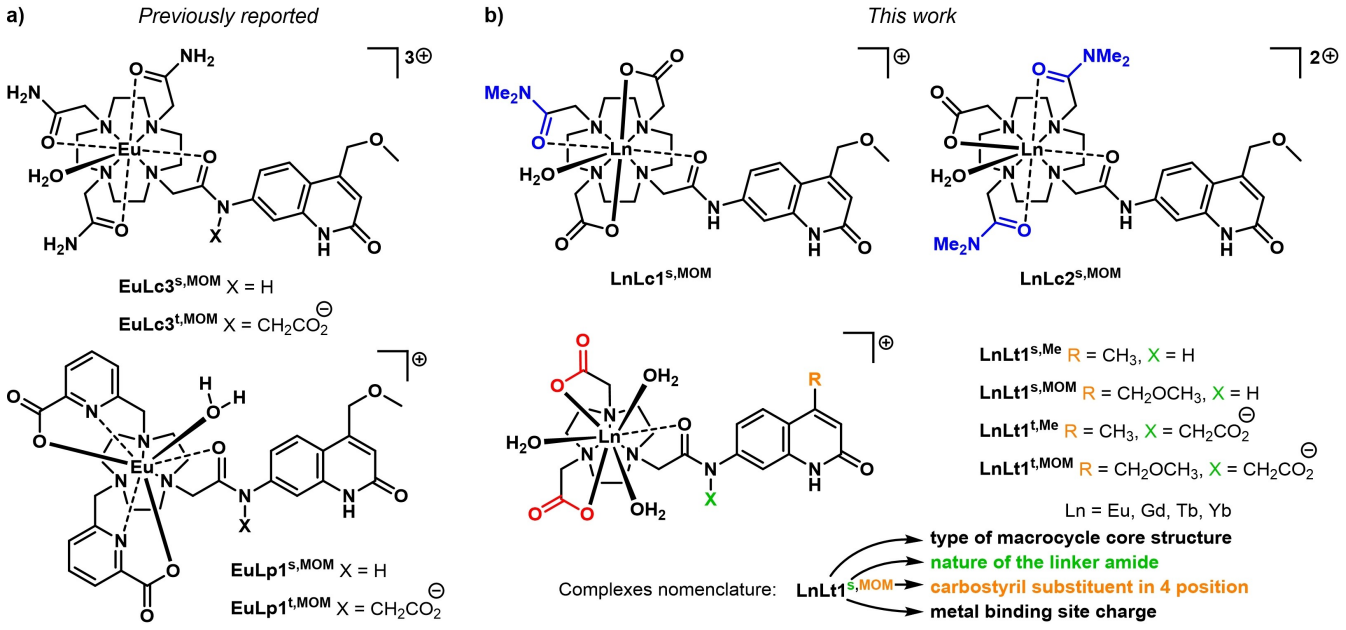

Figure 2. a) Complexes for which the effects of fluoride binding were studied previously (**EuLc3**$^{s/t,MOM}$) and those that are studied here (**EuLp1**$^{s/t,MOM}$). b) New structures prepared for this work. Complex names include macrocyclic core (**c** = cyclen, **p** = picolinate-appended TACN, **t** = TACN), overall charge of the metal binding site (**1**–**3**, indicated in the top right corner of each complex structure), secondary (^{s}) or tertiary (^{t}) amide linker and 4-substitutent of the carbostyril antenna (^{Me} or ^{MOM}).

© 2022 The Authors. Analysis & Sensing published by Wiley-VCH GmbH.

Research Article
doi.org/10.1002/anse.202200015
Chemistry Europe
European Chemical Societies Publishing

TACN-based ligands with two carboxylate donors were prepared; 4-Me or 4-MOM-substituted antennae were attached either through secondary (**Lt1**^{s,R}) or tertiary (**Lt1**^{t,R}) amide linkers. These structures resemble previously reported octadentate ligands equipped with two bidentate picolinate donors (**Lp1**$^{s/t,R}$). The pyridines in **LnLp1**^{s,R} could quench the antenna excited state via PeT.[12] In tertiary amide-linked **LnLp1**^{t,R} (R = Me, MOM and CF_3) Ln(III) luminescence was restored to the levels seen in cyclen-based complexes due to increased η_{sens}.[13] **LnLt1** complexes were not expected to be highly luminescent due to quenching by the up to 3 inner-sphere water molecules.[14] Their inclusion in this study is motivated by the structural variety they introduce, as well as the lack of intraligand PeT. Ligand labels indicate the core structure (**c**, **p**, **t**) and the overall charge of the metal binding site (**1**, **2**, or **3**) rather than the overall charge of the complex (from 0 to +3, Figure 2). The latter is pH-dependent,[11d,e] furthermore, the negatively charged amide substituent has been shown to have only a small influence on the ligand electronic properties.[8]

The second group consists of cyclen-based molecules that are functionalized with three coordinating pendant arms and a 4-methoxymethylcarbostyril antenna. The pendant arms present a *N,N*-dimethylamide and two methylcarboxylate donors (**Lc1**^{s,MOM}) or one methylcarboxylate and two *N,N*-dimethylamide groups (**Lc2**^{s,MOM}). Ln(III) complexes of analogous ligands with primary amide donor groups have been studied before.[6] Amide methylation was expected to reduce N–H quenching of the Eu(III) excited state. Methylation would also influence the Eu(III)/Eu(II) reduction potential, and thus the contribution of PeT.[6]

Synthesis

TACN-based ligands and their complexes were synthesized by one of the two routes as shown in Scheme 1. **6**^{t,MOM} was accessed by monoalkylation of TACN (**1**) with chloroacetylated carbostyril **2**^{t,MOM} to yield **3**^{t,MOM} (60%), which was dialkylated with *tert*-butyl bromoacetate **4** (Scheme 1, left). This route gave substantial quantities of N-alkylated carbostyril byproducts and a smaller yield of **6**^{t,MOM} (29%), which could be avoided by the more convergent route shown in Scheme 1, right.

Disubstituted TACN **5** was alkylated with **2**^{s,R} or **2**^{t,Me} forming **6**^{s,R} or **6**^{t,Me}, respectively, with more than 53% yield. The *tert*-butyl esters of the latter compounds were cleaved by exposure to a mixture of TFA and CH_2Cl_2 (1:1). The volatile components were removed, and the crude product was dried under vacuum. Residual TFA had to be carefully removed as its presence was detrimental to the stabilities of the final complexes. Thus, crude ligands **Lt1**$^{s/t,R}$ were dissolved in a minimum amount of MeOH and triturated with Et_2O, affording the pure products in good yields (57–65%). Heating the ligands at 45 °C in an equimolar mixture of H_2O and EtOH with a slight excess of $LnCl_3$ (Ln = Eu, Gd, Tb and Yb) and 2 or 3 equiv. of NaOH (1 M, aq.) quantitatively yielded pure complexes **LnLt1**$^{s/t,R}$ that were used after evaporation of the solvent and drying under vacuum.

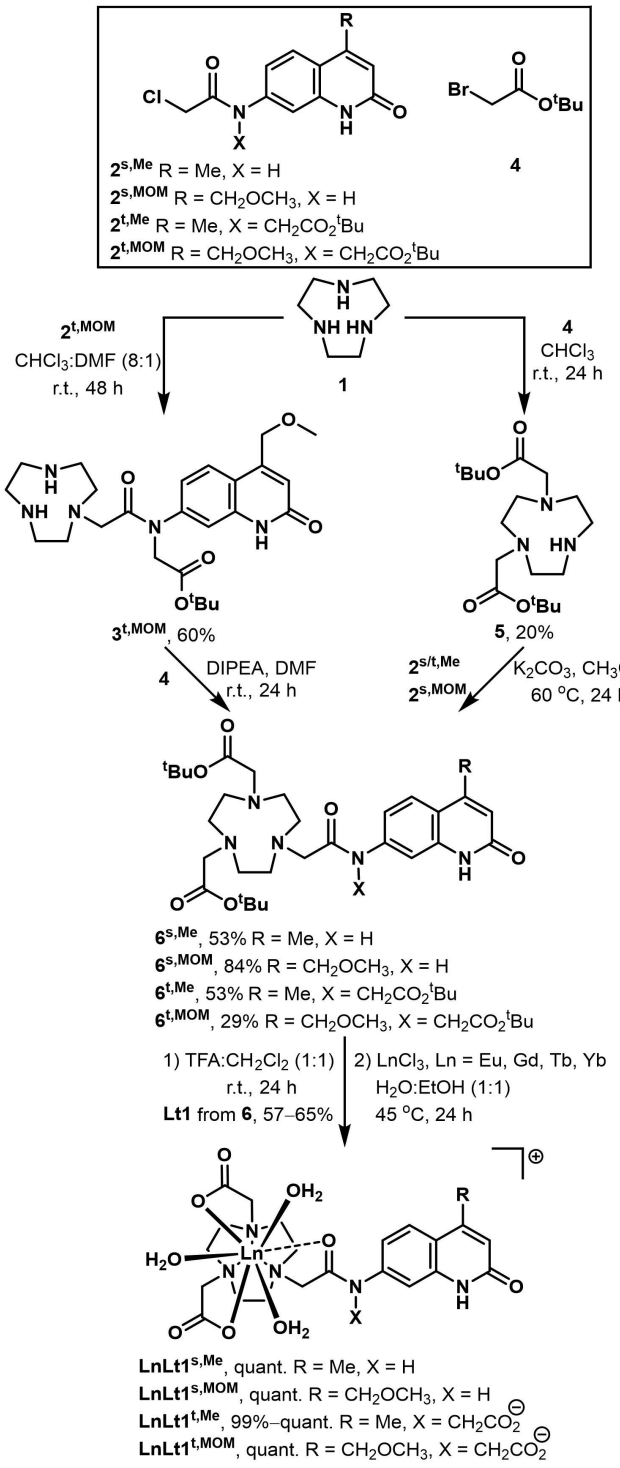

Scheme 1. Synthesis of **LnLt1**.

The two sets of cyclen-based complexes were synthesized as shown in Scheme 2. Ligand precursors **8** and **9** were mono- and dialkylated with *N,N*-dimethyl bromoacetamide (**7**) to quantitatively yield **10** and **11**, respectively. Cleavage of the ^{t}Bu- and Et-groups under acidic (TFA) and basic (NaOH) conditions gave **Lc1**^{s,MOM} (58%) and **Lc2**^{s,MOM} (98%), respectively. Ln(III) complexation in the presence of 2 and 1 equiv. of NaOH (1 M, aq.) in the reaction mixtures yielded **LnLc1**^{s,MOM} and

© 2022 The Authors. Analysis & Sensing published by Wiley-VCH GmbH.

Research Article
doi.org/10.1002/anse.202200015
Chemistry Europe
European Chemical Societies Publishing

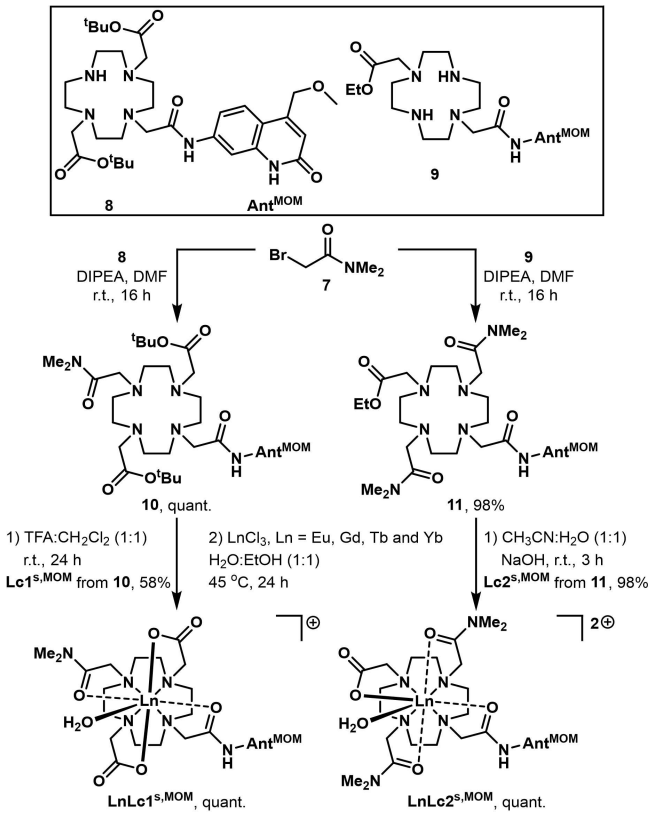

Scheme 2. Synthesis of **Lc1,2**^{s,MOM} and their Ln(III) complexes.

LnLc2^{s,MOM} (Ln = Eu, Gd, Tb and Yb), respectively, with full consumption of the starting materials and high yields.

Synthetic protocols and characterization of new compounds are given in the Supporting Information. Characterization data were consistent with the assigned structures. Further support for the identities of **6**^{t,Me} and **Lt1**^{t,MOM} were provided by single crystal X-ray crystallography (Figure S1, Table S1, deposition number 2157750 (for **Lt1**^{t,MOM}) contains the supplementary crystallographic data for this paper). These data are provided free of charge by the joint Cambridge Crystallographic Data Centre and Fachinformationszentrum Karlsruhe Access Structures service www.ccdc.cam.ac.uk/structures.

Paramagnetic ^{1}H NMR spectroscopy

Ln(III) complex structures in solution were studied with paramagnetic ^{1}H NMR spectroscopy. The Eu(III) and Yb(III) complexes of cyclen derivatives are known to adapt either square antiprismatic (SAP) or twisted SAP (TSAP) coordination environment of the metal centre,[15] which can be identified from the diagnostic axial CH_2 proton signals of the 12-membered ring. The ^{1}H spectra of **EuLc1**^{s,MOM} and **EuLc2**^{s,MOM} in CD_3OD at 0 °C displayed signals attributable to SAP (34.35–39.12 and 31.11–40.03 ppm) and TSAP (14.92–19.63 and 14.21–14.63 ppm) isomers. The ratios of TSAP:SAP were 1:0.54 and 1:0.36 for **EuLc1**^{s,MOM} and **EuLc2**^{s,MOM}, respectively (Figures S2–4). The analogous primary amides also displayed mixtures of SAP and TSAP conformers, the TSAP:SAP ratios were 2.5 and 1.8-fold smaller than that in **EuLc1**^{s,MOM} and **EuLc2**^{s,MOM} (1:0.22 and 1:0.20).[6] The higher proportion of the TSAP isomer in complexes with tertiary amides is probably related to the higher steric demand of the *N*-methyl substituents, which altered the chirality of the pendant arms layout.[16] The Yb(III) complexes in D_2O at 10 °C showed the presence of only SAP species (Figures S5–7, 109.50–122.32 and 108.10–123.41 ppm for **YbLc1**^{s,MOM} and **YbLc2**^{s,MOM}, respectively). The presence of only SAP isomers in the solutions of the Yb(III) complexes (Figure 3) might be explained with Yb(III) having a smaller ionic radius than Eu(III),[17] as the distortion of the coordination polyhedron is also affected by the size of the Ln(III).[18]

The ^{1}H NMR spectrum of **EuLt1**^{t,R} in D_2O showed ~15–16 signals indicating the presence of a single conformer in solution, as there are 15 and 16 theoretically expected resonances for **EuLt1**^{t,Me} and **EuLt1**^{t,MOM}, respectively (4 aromatic CH, 10–11 aliphatic CH_2 and CH_3 protons, Figures S8–9). Heating a solution of **EuLt1**^{t,MOM} to 50 °C slightly displaced and separated ^{1}H chemical shifts, possibly due to paramagnetic induced shifts (Figure S10).[19] From the relative integral ratios, the 4 most deshielded signals were assigned to 4 aromatic CH protons (8.33, 7.84, 7.57 and 7.20 ppm), while the other signals were ascribed to CH_3 (3.89 ppm) and CH_2 protons (5.25 ppm and from 3.50 to −3.34 ppm). The COSY NMR spectrum of **EuLt1**^{t,MOM} in D_2O shows 6 well-resolved ^{1}H-^{1}H couplings, out of which 1 cross-peak corresponds to a pair of adjacent aromatic protons from the carbostyril antenna, while the rest are the interactions between neighboring CH_2 hydrogen atoms in the TACN moiety (Figure S11). The solution structure of **EuLt1**^{t,MOM} appears to contain one major conformer, while the picolinate-functionalized **EuLp1**^{t,MOM} had two species in D_2O also at high temperature.[13] Since there are only 6 donor atoms provided by the ligand to coordinate Eu(III) in the former complex, the remaining 3 coordination sites are filled with 3 H_2O molecules

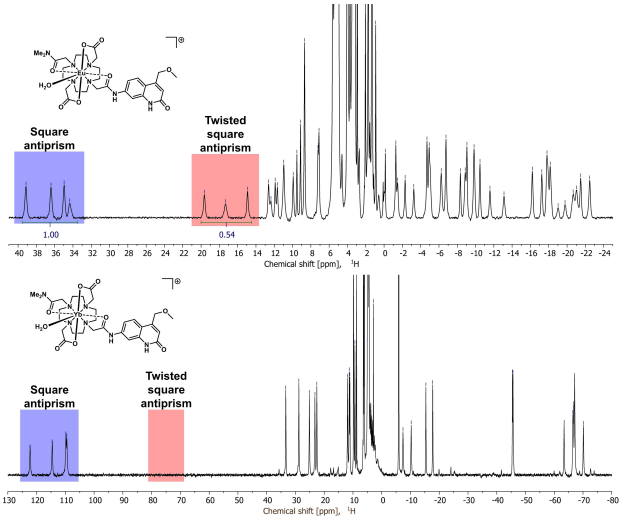

Figure 3. ^{1}H NMR spectra (400 MHz) of **EuLc1**^{s,MOM} (top) and **YbLc1**^{s,MOM} (bottom) measured at 0 °C in CD_3OD and at 10 °C in D_2O, respectively. The highlights in blue and red show the regions diagnostic for the CH_2 cyclen ring signals of the SAP and TSAP isomers, respectively.

© 2022 The Authors. Analysis & Sensing published by Wiley-VCH GmbH.

Research Article
doi.org/10.1002/anse.202200015

Chemistry Europe
European Chemical Societies Publishing

(*vide infra*). In contrast, the coordination polyhedron of **EuLp1^{t,MOM}** is very distorted due to the steric demand of the two picolinates, resulting in interconverting species of different TACN ring helicities in solution.[13] We could not record well-resolved ^{1}H NMR spectra of **EuLt1^{s,R}** and **YbLt1** complexes in D_2O or CD_3OD.

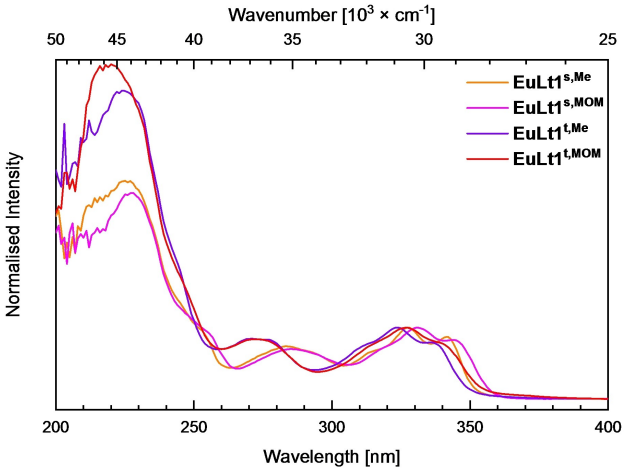

Figure 4. Normalized and superimposed absorption spectra of **EuLt1**. [**EuLt1**] = 10–20 μM in aqueous 10 mM PIPES buffer solutions at pH = 6.5.

Photophysical characterization

Absorption, excitation, and emission spectra of new complexes (Figure 2b) were recorded in PIPES-buffered (pH 6.5, 10 mM) aqueous solutions with ≈10–20 μM concentration of the complexes (Figures S13–24). The absorption spectra of **LnLt1^{s,R}** and **LnLt1^{t,R}** were similar, with C=O n-π* and antenna π-π* absorptions at ~260–290 nm and at ~323–325 nm for **LnLt1^{t,R}**, and at 265–295 nm and at 327–330 nm for **LnLt1^{s,R}** (Figure 4). Antenna substitution and the amide linker influenced the spectra only modestly. The largest difference was the 12 nm blue-shift of the 284 nm band due to the replacement of the secondary amide linker in **LnLt1^{s,R}** with a tertiary one in **LnLt1^{t,R}**. The absorption profiles of **LnLc1^{s,MOM}** and **LnLc2^{s,MOM}** were almost identical, with only a small growth at 265–310 nm for **LnLc2^{s,MOM}** (Figure S25). The spectra of the same ligand with different Lns were superimposable (Figures S26–28). Thus, the new complexes have absorption features that are similar to previously reported ones lacking pyridines, such as **LnLc3^{s,R}**[6] and **LnLc0^{t,R}**.[8,11e]

Excitation into the absorption bands at 324, 327, 329 and 330 nm yielded both antenna and Ln(III) (Ln = Tb, Eu) emission (Figures 5, S29–30). Antenna fluorescence consisted of two bands. The emission band at λ_{em} = 365 and 375 nm has previously been observed in other complexes carrying the same antennae with 4-Me and 4-MOM substituents, respectively. The second band was located at λ_{em} = 417 and 445 nm for **EuLt1$^{s/t,Me}$** and **EuLt1$^{s/t,MOM}$**, respectively. The steady-state

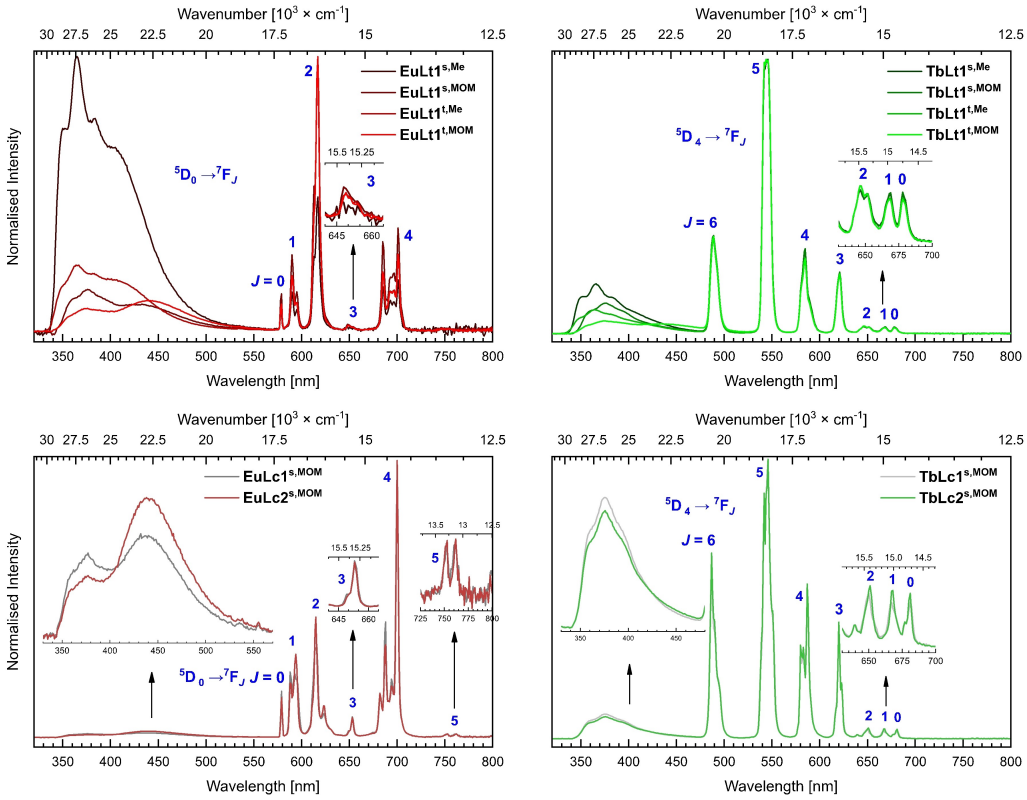

Figure 5. Normalized and superimposed steady-state emission spectra of **EuL** (left) and **TbL** complexes (right). [**LnL**] = 10–20 μM in aqueous 10 mM PIPES buffer solutions at pH 6.5 measured with λ_{ex} = 324, 327, 329 and 330 nm for **LnLt1^{t,Me}**, **LnLt1^{t,MOM}** and **LnLt1^{s,Me}**, **LnLt1^{s,MOM}**, **LnL1,2^{s,MOM}** respectively.

© 2022 The Authors. Analysis & Sensing published by Wiley-VCH GmbH.

Research Article
doi.org/10.1002/anse.202200015
Chemistry Europe
European Chemical Societies Publishing

emission spectra of **EuLc1,2^{s,MOM}** also contained this second red-shifted band (λ_{em} = 442 nm) in addition to the original antenna emission (λ_{em} = 376 nm). The lowest-energy absorption band was blue-shifted in water compared to DMF:water and pure DMF solutions, while in H_2O the emission from the lower-energy band became more intense compared to what was seen in the less polar solvents. These observations are consistent with the red-shifted band arising from an internal charge transfer (ICT) state that is better stabilized by more polar solvents (Figures S31–40).[20] The λ_{em} of the ICT peak is more sensitive to the carbostyril substituent than that of the locally excited (LE) state (Figures S41–42). The linker has no influence on the ICT emission and only a small effect on the LE state energies, and a meaningful one on Φ_{ICT}. **LnLt1^{t,MOM}** Φ_{ICT} decreased linearly with the Ln(III) Lewis acidity, but not the Φ_{ICT} of **LnLt1^{t,Me}** and **LnLt1^{s,R}** (Figures S43–44).

Ln(III) excitation spectra were similar to the UV-Vis absorption spectra showing that Ln(III) emission is sensitized by the antenna (Figures S14, 16, 18, 20, 22, 24). Eu(III) emission peaks were at 579, 590, 617, 649, and 701 nm, corresponding to the $^5D_0 \rightarrow {}^7F_J$ transitions (J = 0–4), while the Tb(III) spectra displayed peaks at 489, 544, 585, 621, 646, 668, and 678 nm, corresponding to the $^5D_4 \rightarrow {}^7F_J$ (J = 6–0) transitions. The shapes of the **LnLc1,2^{s,MOM}** Ln(III) emission spectra differed from those of their **LnLt1** analogues due to their different geometries. Specifically, the $\Delta J = 4$ transition (700 nm) was the most intense for **EuLc1,2^{s,MOM}**, while for **EuLt1** it was the $\Delta J = 2$ transition (614 nm). The $^5D_0 \rightarrow {}^7F_5$ transition was absent in the **EuLt1** emissions but was present in the **EuLc1,2^{s,MOM}** spectra. In case of Tb(III) complexes, the Stark splitting of emission bands in **TbLc1,2^{s,MOM}** increased compared to their **TbLt1** analogues.

The emission lifetimes (τ_{obs}) of the Eu(III) and Tb(III) complexes were measured in PIPES-buffered H_2O (τ_{H2O}) and D_2O (τ_{D2O}, Table 1). **EuLt1** have very similar τ_{obs} in the aqueous buffer, ~0.27 ms. **EuLc1,2^{s,MOM}** had τ_{obs} ~0.60 ms which is comparable to τ_{obs} of other cyclen-based emitters, and slightly longer than those of analogous complexes carrying $CH_2C(O)NH_2$ groups due to the absence of the N–H bonds.[6] In D_2O, the lifetimes of Eu(III) TACN and cyclen-based complexes were ~1.55 and ~1.93 ms, respectively. For **TbLt1**, τ_{obs} varied more: τ_{H2O} and τ_{D2O} ranged from 0.60–0.98 ms and 1.14–2.31 ms, respectively. Furthermore, the Tb(III) luminescence was oxygen sensitive, which is consistent with thermal back energy transfer (Figures S45–46, Table S6). In PIPES-buffered H_2O and D_2O for **TbLc1,2^{s,MOM}** τ_{obs} were 0.94 and 1.41 ms, respectively.

Table 1. Ln(III) emission lifetimes and hydration states of **LnL**.[a]

Complex	τ_{H2O} [ms]	τ_{D2O} [ms]	q[b][c]
EuLt1^{s,Me}	0.259	1.47	3.4
EuLt1^{s,MOM}	0.265	1.54	3.4
EuLt1^{t,Me}	0.266	1.51	3.4
EuLt1^{t,MOM}	0.267	1.55	3.4
EuLc1^{s,MOM}	0.601	2.03	1.0
EuLc2^{s,MOM}	0.602	1.83	1.0
TbLt1^{s,Me}	0.730	0.873	*n.d.*
TbLt1^{s,MOM}	0.643	0.774	*n.d.*
TbLt1^{t,Me}	0.920	1.67	2.1
TbLt1^{t,MOM}	0.930	2.25	2.9
TbLc1^{s,MOM}	0.904	1.42	*n.d.*
TbLc2^{s,MOM}	0.979	1.40	*n.d.*

[a] [**LnL**] = 10–20 μM in 10 mM PIPES buffered H_2O or D_2O at pH 6.5 and pD 6.9. [b] Calculated using the equation $q = 5(1/\tau_{H2O} - 1/\tau_{D2O} - 0.06)$ for Tb, and $q = 1.2(1/\tau_{H2O} - 1/\tau_{D2O} - 0.25 - m \cdot 0.075)$, where m is the number of nearby N–H oscillators.[21c] [c] *n.d.*: values could not be determined due to BET.

Ln(III) luminescence in previously reported complexes with the same antennae was sensitized predominantly through the antenna triplet (T_1), with minor contribution from the singlet excited state (S_1).[11d,e] The T_1 were determined from the 0→0 phonon transitions of the emission spectra of **GdL** recorded at 77 K,[22] and were at ~23000 cm^{-1} for **GdLt1^{t,R}**. The T_1 for the compounds with secondary amide linkers were of lower energy, ranging from 22900 cm^{-1} for **GdLt1^{s,Me}** to 22570 ± 50 cm^{-1} for **GdLt1^{s,MOM}** and **GdLc1,2^{s,MOM}** (Figures S47–48). The biggest difference in T_1 levels between the complexes of different binding sites (**Lc** vs **Lt**) but same antenna and linker amide was within 100 cm^{-1} indicating negligible influence of the macrocycle size on antenna excited state levels (Table S7).[11d,e] Thus, the antennae have T_1 that are well-placed for energy transfer to Eu(III). Those complexes, however, that have antennae with T_1 within ~2000 cm^{-1} of the $^5D_4$ (20600 cm^{-1}) Tb(III) excited state, are expected to participate in thermal energy back transfer, and thus have oxygen-sensitive Tb(III) luminescence.

The ligand and metal-centered quantum yields were determined using the optically dilute method with quinine sulfate[23] as the fluorescence standard (Table 2). As in the case of previously reported emitters, tertiary amide-linked antennae were better at both Eu and Tb sensitization than secondary amide-linked ones. For example, the q = 3 complex **TbLt1^{t,MOM}** had Φ_{Tb} = 24.9%, a value similar to the Φ_{Tb} of the q = 1 complexes **TbLc1^{s,MOM}** (Φ_{Tb} = 22.5%) and **TbLc2^{s,MOM}** (Φ_{Tb} = 24.3%). The above three ligands yielded Eu complexes with the highest Φ_{Eu}, ~4%. The much lower Φ_{Ln} of the Eu(III) emitters compared to the analogous Tb species is due to several factors, including the lower intrinsic quantum yield of Eu(III), the higher sensitivity of the Eu(III) excited state to X–H quenching, and especially in emitters with secondary amide-linked antennae, PeT quenching.

In the analysis of antenna photophysics, the Φ_L values of the Gd(III) chelates were used as the reference. Gd(III) is neither photoactive under the experimental conditions nor reducible by the excited antennae ($E(Gd^{III}/Gd^{II}) = -3.9$ V)).[24] Thus, antenna excited states are not depleted by singlet-mediated energy transfer, which is possible for Ln(III) with excited states of comparable energy levels (Ln = Eu, Tb), or by PeT, which is feasible for reducible Ln(III) (Ln = Eu, Yb). Where both LE and ICT states were emitting, they were quantified separately as Φ_L and Φ_{ICT}, respectively, and their sum is reported as $\Phi_{L,tot}$.

© 2022 The Authors. Analysis & Sensing published by Wiley-VCH GmbH.

Research Article
doi.org/10.1002/anse.202200015

Table 2. Emission quantum yields of **LnL**.[a]

Complex	Φ_L [%] [b]	Φ_{ICT} [%] [b]	$\Phi_{L,tot}$ [%] [b]	Φ_{Ln} [%] [b]
GdLt1^{s,Me}	6.2	1.1	7.3	–
GdLt1^{s,MOM}	6.2	0.46	6.7	–
GdLt1^{t,Me}	4.4	1.1	5.5	–
GdLt1^{t,MOM}	4.3	3.1	7.4	–
GdLc1^{s,MOM}	7.1	–	7.1	–
GdLc2^{s,MOM}	6.4	–	6.4	–
TbLt1^{s,Me}	4.6	1.1	5.7	9.9
TbLt1^{s,MOM}	4.9	0.66	5.6	15.3
TbLt1^{t,Me}	4.5	1.3	5.8	17.7
TbLt1^{t,MOM}	4.0	3.4	7.4	24.5
TbLc1^{s,MOM}	4.9	–	4.9	22.5
TbLc2^{s,MOM}	4.8	–	4.8	24.3
EuLt1^{s,Me}	2.0	1.2	3.2	0.30
EuLt1^{s,MOM}	0.61	0.45	1.1	1.1
EuLt1^{t,Me}	1.7	1.2	2.9	1.6
EuLt1^{t,MOM}	2.1	2.7	4.8	4.1
EuLc1^{s,MOM}	0.24	0.38	0.62	4.3
EuLc2^{s,MOM}	0.17	0.53	0.70	3.9
YbLt1^{s,Me}	2.8	1.4	4.2	–
YbLt1^{s,MOM}	3.7	0.66	4.4	–
YbLt1^{t,Me}	4.1	1.3	5.4	–
YbLt1^{t,MOM}	3.8	4.5	8.3	–
YbLc1^{s,MOM}	5.6	–	5.6	–
YbLc2^{s,MOM}	5.0	–	5.0	–

[a] [**LnL**] = 10–20 μM in 10 mM PIPES buffered H_2O at pH 6.5. [b] Relative to quinine sulfate ($\Phi = 0.59$) in H_2SO_4 (0.05 M).[23]

TbLt1^{t,R} had Φ_L, Φ_{ICT}, and $\Phi_{L,tot}$ essentially identical to what was obtained for Gd(III) analogues. Secondary amide-linked **TbLt1^{s,R}**, however, had lower Φ_L, and $\Phi_{L,tot}$ but unchanged Φ_{ICT}, which is consistent with energy transfer (ET) happening from the antenna S_1, but not from the lower-energy ICT state. Tb(III) has a number of closely-spaced excited states above 26000 cm^{-1}[25] to which ET from the high-energy LE states should be fast. The ICT state can only engage in ET to $^5D_4$; the gap of >5000 cm^{-1} makes such a process slow.

EuL have significantly lower $\Phi_{L,tot}$ than the analogous **GdL**, which can be due to both ET from S_1 and PeT. While changes are small, Φ_L appears to be more affected than Φ_{ICT}. PeT quenching of the antenna excited state is also consistent with the lower Φ_L seen for **YbL**. Yb(III) lacks energetic excited states that could participate in ET with the antenna LE or ICT states, thus only PeT contributes to the antenna fluorescence quenching.

Eu(III) emitters were then exposed to an excess of fluoride or cyanide and the changes in the antenna and Eu(III) emissions were evaluated. Anion binding and control experiments were performed in 10 mM aqueous or D_2O TRIS buffer solutions at pH 8.1 and pD 8.5[26] to avoid the formation of HCN when working with potassium cyanide (KCN). Φ_{Ln}^{Ln} and η_{sens} of **EuL** in the absence and presence of anions were determined using Eqs 2 and 3.[27]

$$1/\tau_{rad} = A_{MD,0} \cdot n^3 \cdot (I_{tot}/I_{MD}) \quad (2)$$

$$\Phi_{Ln}^{Ln} = \tau_{obs}/\tau_{rad} \quad (3)$$

Φ_{Ln} is proportional to η_{sens} and Φ_{Ln}^{Ln}, and the latter is inversely proportional to τ_{rad}. The TACN-based complexes have τ_{rad} ~3 ms irrespective of whether they have picolinate donors or carboxylate-based ones. The similarity of τ_{rad} may hint at the similar coordination geometries of **EuLt1** and **EuLp1**. **EuLt1**, however, had Φ_{Ln}^{Ln} half of that for **EuLp1**, which is due to the former having 2 more inner-sphere water molecules. The cyclen-based complexes have τ_{rad} typical of such species (~ 5 ms).[6,8, 11e] Values for η_{sens} were higher for tertiary amide-linked species than for those with a secondary amide linker. Sensitization was least efficient in emitters with secondary amide-linked antennae subject to efficient PeT quenching by pyridines[12] (**EuLp1^{s,MOM}**) or readily reducible Eu(III)[6] (**EuLc3^{s,MOM}**). It is worth noting that the parameters in Table 3 are sensitive to the experimental conditions. Previously reported τ_{rad}, Φ_{Ln}^{Ln}, and η_{sens} values of **EuLp1^{s,MOM}** and **EuLc3^{s,MOM}** with secondary amide linked antennae in aqueous PIPES buffer at pH = 6.5[6,12] are different from the values listed here due to the pH-sensitivity of the emission (Figures S49–59). The largest loss of emission was for secondary amide-linked complexes at pH > 9, tertiary amide-linked ones were essentially unchanged until pH = 10. The loss of Eu emission at higher pH was reversible. Under acidic conditions the complexes of the hexadentate **Lt** ligands were unstable (Figures S56–57). Buffer components may influence Ln(III) luminescence.[28] While TRIS has recently been reported to interact less with hydrated Eu(III) than PIPES, it has a clear influence on **EuLc3^{s,MOM}** (Figure S49). τ_{H2O} (0.188 ms) and τ_{D2O} (0.611 ms) are both much shorter for this complex than for the other cyclen-based species, or the same complex in PIPES[6] (> 0.5 ms and > 1.6 ms, respectively, Table S10).

The addition of an excess of potassium fluoride (KF) increased Φ_{Ln} of all the Eu(III) complexes (Tables 4 and 5). Analysis of the corrected spectra using Eqs. 2 and 3 showed that the turn-on response was due to two factors. First, fluoride replaced at least some of the water molecules in all the hydrated complexes, in some cases all 3 aqua ligands were swapped for fluorides (e.g. **EuLt1^{s,R}**, **EuLt1^{t,R}**). Water displacement in cationic complexes with fluoride is well-established.[9a,c, 30] Comparison of the emission spectra and τ_{rad} before and after KF addition showed that ligand exchange altered τ_{rad} to a small extent, but in general the spectral shapes were little effected,

Table 3. Eu(III)-based photophysical properties of **EuL**.[a]

Complex	τ_{rad} [ms] [b]	Φ_{Ln}^{Ln} [%] [b]	η_{sens} [%] [b]
EuLt1^{s,Me}	3.21	7.87	4.33
EuLt1^{s,MOM}	3.43	7.31	16.3
EuLt1^{t,Me}	3.13	8.70	19.2
EuLt1^{t,MOM}	3.05	8.90	52.4
EuLp1^{s,MOM}	2.86	14.8	13.7
EuLp1^{t,MOM}	2.93	17.6	35.1
EuLc1^{s,MOM}	5.08	11.6	30.1
EuLc2^{s,MOM}	5.07	10.0	27.1
EuLc3^{s,MOM}	5.18	3.62	7.89
EuLc3^{t,MOM}	4.65	10.9	33.1

[a] [**EuL**] = 10–20 μM in 10 mM aqueous TRIS buffer solutions at pH = 8.1. [b] Determined using eqs. 2 and 3, I_{tot}/I_{MD} is integral ratio of the total metal-centered corrected emission spectrum (521–800 nm) and the $^5D_0 \rightarrow {}^7F_1$ band (582–603 nm), $A_{MD,0} = 14.65\ s^{-1}$, the refractive index is $n = 1.333$,[29] and $\tau_{obs} = \tau_{H2O}$ in water.

© 2022 The Authors. Analysis & Sensing published by Wiley-VCH GmbH.

Research Article
doi.org/10.1002/anse.202200015
Chemistry Europe
European Chemical Societies Publishing

Table 4. Φ_{Ln} and change in Φ_{Ln} of **EuL** upon KF and KCN addition.[a]

Complex	Φ_{Ln}(KF) [b]	Φ_{Ln}(KCN) [b]
EuLt1^{s,Me}	2.06 (×6.0)	0.15 (×0.45)
EuLt1^{s,MOM}	3.30 (×2.8)	0.44 (×0.37)
EuLt1^{t,Me}	7.84 (×4.7)	1.04 (×0.62)
EuLt1^{t,MOM}	16.0 (×3.4)	1.24 (×0.27)
EuLp1^{s,MOM}	13.8 (×6.8)	1.08 (×0.53)
EuLp1^{t,MOM}	18.5 (×3.0)	6.01 (×0.97)
EuLc1^{s,MOM}	6.19 (×1.8)	1.46 (×0.42)
EuLc2^{s,MOM}	10.3 (×3.8)	0.35 (×0.13)
EuLc3^{s,MOM}	7.20 (×25.2)	0.05 (×0.16)
EuLc3^{t,MOM}	13.2 (×3.7)	2.82 (×0.78)

[a] [**LnL**] = 10 μM in 10 mM TRIS buffered H_2O at pH 8.1 with 1 M (**EuLt**) or 0.1 M KF or KCN. [b] Relative to quinine sulfate ($\Phi = 0.59$) in H_2SO_4 (0.05 M).[23] In parentheses the change relative to the solution without KF or KCN.

Table 5. Eu(III)-based photophysical properties of **EuL-F**.[a]

Complex	τ_{rad} [ms] [b]	Φ_{Ln}^{Ln} [%] [b]	η_{sens} [%] [b]	Δq
EuLt1^{s,Me}-F	4.06 (×1.26)	19.8 (×2.52)	10.4 (×2.40)	−3.1
EuLt1^{s,MOM}-F	4.13 (×1.20)	19.4 (×2.65)	17.0 (×1.04)	−3.1
EuLt1^{t,Me}-F	3.72 (×1.19)	21.7 (×2.49)	36.1 (×1.88)	−2.7
EuLt1^{t,MOM}-F	3.74 (×1.23)	21.8 (×2.45)	73.3 (×1.40)	−2.8
EuLp1^{s,MOM}-F	3.71 (×1.30)	28.9 (×1.95)	47.8 (×3.49)	−1.5
EuLp1^{t,MOM}-F	3.47 (×1.18)	31.1 (×1.77)	59.5 (×1.70)	−1
EuLc1^{s,MOM}-F	5.04 (×0.99)	16.1 (×1.39)	38.4 (×1.28)	−0.6
EuLc2^{s,MOM}-F	5.06 (×1.00)	21.3 (×2.13)	48.4 (×1.79)	−1.1
EuLc3^{s,MOM}-F	4.75 (×0.92)	20.0 (×5.52)	36.1 (×4.58)	−3.7
EuLc3^{t,MOM}-F	4.78 (×1.03)	20.9 (×1.92)	63.0 (×1.90)	−1

[a] [**EuL**] was 10–20 μM in 10 mM aqueous TRIS buffer solutions at pH 8.1 with 1 M (**EuLt**) or 0.1 M KF. [b] Determined using eqs. 2 and 3, I_{tot}/I_{MD} is integral ratio of the total metal-centered corrected emission spectrum (521–800 nm) and the $^5D_0 \rightarrow {}^7F_1$ band (582–603 nm), $A_{MD,0} = 14.65\ s^{-1}$, the refractive index is $n = 1.333$,[29] and $\tau_{obs} = \tau_{H2O}$ in water. In parentheses the change relative to the solution lacking KF.

and the fluoride complexes likely have geometries similar to the hydrated parents (Figures S63–72). Therefore, the increase in Φ_{Ln}^{Ln} can be explained by the removal of the inner sphere O–H oscillators. The second factor was the stabilization of the +3 oxidation state of Eu by the anionic fluoride ligand, which can be quantified by the changes in η_{sens}. Secondary amide-linked complexes experienced a larger increase in η_{sens} than the analogous tertiary amide-linked ones. This is expected, as the emission of the former are more efficiently quenched by antenna-to-Eu(III) PeT. For complexes with the same macrocyclic core (e.g. **Lc**) the more positively charged the complex the more η_{sens} is improved by fluoride binding, which is consistent with fluoride interfering a quenching pathway that is more prominent for more reducible Eu(III).

The largest turn-on response (25-fold) was seen for **EuLc3^{s,MOM}-F**. For this species the effects on both Φ_{Ln}^{Ln} and η_{sens} are exceptionally large. The former parameter increases 5.52-fold, a change that is twice of what was obtained by the replacement of 3 inner-sphere H_2O ligands in **EuLt1^{s,MOM}**. The increase in η_{sens} is also the largest in this group of emitters, or what was obtained for the same complex in PIPES buffer, which provides further support for the non-innocence of the TRIS buffer in the case of **EuLc3^{s,MOM}**. A state-of-the-art fluoride probe based on H_2O ligand displacement showed a 9-fold increase in Eu(III) luminescence in pure water,[9a] which is slightly higher than what was seen for the other emitters studied here (Table 4).

To our surprise, cyanide addition under the same conditions quenched Φ_{Ln} in all cases (Table 4). Determination of the q values of the cyanide complexes showed the displacement of some or all of the Eu-bound water molecules in all but one compound (Table 6). On average $|\Delta q|$ was smaller than upon fluoride addition (Table 5), which is likely due to cyanide being a softer anion than fluoride and thus having a lower affinity for the hard Eu(III) centers. Lower q, however, was not always accompanied by higher Φ_{Ln}^{Ln}. Furthermore, increases in Φ_{Ln}^{Ln} could not compensate for the dramatic cyanide-induced decreases in η_{sens}, which resulted in overall lower Φ_{Ln}.

The reasons for the lower η_{sens} are unclear, and are likely different for the different types of complexes. Cyanide addition to **EuLc^s** red-shifted antenna absorptions; tertiary amide-linked antennae in **Lc** ligands were less affected (Figures S63–72). In **Lt**, the changes were similar for both secondary and tertiary amides, and were accompanied by prominent ICT-emissions; $\Phi_{L,tot}$ were higher than without cyanide. In cyclen-based systems the proportion of η_{sens} retained after cyanide addition was smaller for more positively charged complexes: 0.52, 0.18, and 0.09% for **EuLc1**, **EuLc2**, and **EuLc3**, respectively. In these complexes the antenna emission was also quenched. We tentatively propose that in these emitters cyanide interacts with the antenna linker creating a more electron-donating group. Cyanide addition to ketone linkers yielding cyanohydrins is possible, and the resulting adducts have been shown to leave the Ln(III) coordination environment unchanged.[31] Amide linkers were shown to be inert under those conditions, thus cyanohydrin formation is less likely in our case. ^{1}H NMR spectroscopic analyses of the cyanide-containing solutions of diamagnetic **LuLc3^{s,MOM}** and **LuLc3^{t,MOM}** complexes were inconclusive (Figures S75–S79). Even adding as little as 1 equiv. of KCN caused significant line broadening; low temperature measurements (283 K for D_2O) did not resolve the signals. Despite the broadening, the number of signals in the aromatic region (4 peaks) was unchanged, which suggests that the

Table 6. Eu(III)-based photophysical properties of **EuL-CN**.[a]

Complex	τ_{rad} [ms] [b]	Φ_{Ln}^{Ln} [%] [b]	η_{sens} [%] [b]	Δq
EuLt1^{s,Me}-CN	2.76 (×1.26)	10.7 (×1.36)	1.44 (×0.33)	−2.4
EuLt1^{s,MOM}-CN	2.76 (×1.26)	11.1 (×1.52)	3.91 (×0.24)	−2.4
EuLt1^{t,Me}-CN	3.12 (×1.00)	11.5 (×1.32)	9.01 (×0.47)	−1.1
EuLt1^{t,MOM}-CN	2.99 (×0.98)	12.1 (×1.36)	10.3 (×0.20)	−1.2
EuLp1^{s,MOM}-CN	3.19 (×1.12)	10.8 (×0.73)	10.0 (×0.73)	−0.5
EuLp1^{t,MOM}-CN	3.11 (×1.06)	16.8 (×0.95)	35.9 (×1.02)	+1.0
EuLc1^{s,MOM}-CN	4.83 (×0.95)	9.20 (×0.79)	15.8 (×0.52)	0.1
EuLc2^{s,MOM}-CN	4.47 (×0.88)	7.05 (×0.71)	4.92 (×0.18)	0.2
EuLc3^{s,MOM}-CN	3.58 (×0.69)	6.74 (×1.86)	0.69 (×0.09)	−1.3
EuLc3^{t,MOM}-CN	3.97 (×0.85)	11.1 (×1.02)	25.3 (×0.76)	−0.5

[a] [**EuL**] = 10–20 μM in 10 mM aqueous TRIS buffer solutions at pH = 8.05 with 1 M (**EuLt**) or 0.1 M KCN. [b] Determined using eqs. 2 and 3, I_{tot}/I_{MD} is integral ratio of the total metal-centered corrected emission spectrum (521–800 nm) and the $^5D_0 \rightarrow {}^7F_1$ band (582–603 nm), $A_{MD,0} = 14.65\ s^{-1}$, the refractive index is $n = 1.333$,[29] and $\tau_{obs} = \tau_{H2O}$ in water. In parentheses the change relative to the solution lacking KCN.

© 2022 The Authors. Analysis & Sensing published by Wiley-VCH GmbH.

antenna remains intact, although the metal-bound cyanide could indirectly impact the linker and/or the antenna. The resulting species may be less competent in ET (in **EuLt**), or may be more susceptible to PeT (in **EuLc**). The nature of this cyanide adduct is currently under investigation. Finally, **EuLp1^{s,MOM}–CN** gained a Ln-bound water molecule upon KCN addition. Cyanohydrin formation did not alter τ_{H2O} in the ketone-containing **Lc**-type species,[31] which also points towards a non-cyanohydrin product.

Conclusion

Luminescent lanthanide complexes based on structurally diverse macrocyclic ligands were prepared. The ligands were based on three types of macrocycles (cyclen, TACN, TACN with picolinate), had three types of donors (bidentate picolinate, and monodentate carboxylate and carboxamide), two types of linkers connecting the sensitizing antenna to the metal binding site (secondary and tertiary amide), and two sensitizing antennae (4-Me or 4-MOM-substituted 7-aminocarbostyril). Steady-state and time-resolved emission spectroscopy showed that the Eu and Tb complexes were all luminescent and their coordination spheres were completed in aqueous solution by 1–3 water molecules. The antennae were competent sensitizers for Eu and Tb. The Eu complexes had lower overall Φ_{Ln} due to a combination of antenna quenching by PeT and Ln(III) excited state quenching by X–H oscillators. Several Tb emitters had $\Phi_{Ln} > 20\,\%$ including the $q = 3$ complex **TbLt1^{t,MOM}**.

Exposure of the Eu(III) emitters to excess fluoride increased Eu(III) luminescence by up to 25-fold. The turn-on response was due to two distinct mechanisms, the replacement of Eu-bound X–H quenchers by fluoride ligands, and the stabilization of Eu(III) against reduction by the photoexcited antenna. Cyanide elicited a very different response, and quenched the Eu(III) luminescence of every complex, albeit to varying extents: **EuLp1^{t,MOM}** and **EuLc2^{s,MOM}** retained 97 % and 13 % of their emissions, respectively. The mechanism via which cyanide quenches Eu(III) luminescence may be by altering the electronic structure of antenna, which in turn decreases the sensitization efficiency, however, we have not yet been able to identify any covalent adducts between cyanide and the complexes. The exact nature of these changes and how they affect the rate of photoinduced electron transfer and Eu(III) sensitization are under investigation. Future studies are aimed at understanding how and to what extent metal-bound anions can influence the redox properties of the various Ln(III) centers. A range of anions in addition to fluoride and cyanide coordinate effectively to Ln(III), including acetate, lactate, hydrogen carbonate, and hydrogen phosphate.[32] Finally, should these redox effects translate to changes in the luminescent properties, anions of similar shapes and binding modes but different charge densities (e.g. different halides) may be distinguished.

Acknowledgements

*This work was supported by the Swedish Research Council (project grant 2017-04077 for K.E.B.) and the Knut och Alice Wallenbergs Foundation (Dnr: 2018.0066 and Dnr: KAW 2019.0071). We thank Daniel Kocsi for a gift of **EuLp1$^{s/t,MOM}$**.*

Conflict of Interest

The authors declare no conflict of interest.

Data Availability Statement

The data that support the findings of this study are available from the corresponding author upon reasonable request.

Keywords: cyanide · fluoride · lanthanide luminescence · macrocyclic ligands · responsive probes

[1] A. de Bettencourt-Dias, in *Luminescence of Lanthanide Ions in Coordination Compounds and Nanomaterials*, John Wiley & Sons Ltd, **2014**, pp. 1–48.
[2] J.-C. G. Bünzli, *Acc. Chem. Res.* **2006**, *39*, 53–61.
[3] a) S. J. Butler, M. Delbianco, L. Lamarque, B. K. McMahon, E. R. Neil, R. Pal, D. Parker, J. W. Walton, J. M. Zwier, *Dalton Trans.* **2015**, *44*, 4791–4803; b) E. Pershagen, K. E. Borbas, *Coord. Chem. Rev.* **2014**, *273–274*, 30–46; c) J. M. Zwier, N. Hildebrandt, *Rev. Fluoresc.* **2016**, *9*, 17–43; d) D. Parker, J. D. Fradgley, K.-L. Wong, *Chem. Soc. Rev.* **2021**, *50*, 8193–8213; e) S. H. Hewitt, S. J. Butler, *Chem. Commun.* **2018**, *54*, 6635–6647; f) Y. Ning, M. Zhu, J.-L. Zhang, *Coord. Chem. Rev.* **2019**, *399*, 213028.
[4] a) O. Guillou, C. Daiguebonne, G. Calvez, K. Bernot, *Acc. Chem. Res.* **2016**, *49*, 844–856; b) J. Andres, R. D. Hersch, J.-E. Moser, A.-S. Chauvin, *Adv. Funct. Mater.* **2014**, *24*, 5029–5036; c) H. S. Jena, H. Rijckaert, C. Krishnaraj, I. Van Driessche, P. Van Der Voort, A. M. Kaczmarek, *Chem. Mater.* **2021**, *33*, 8007–8017.
[5] J.-C. G. Bünzli, S. V. Eliseeva, in *Lanthanide Luminescence: Photophysical, Analytical and Biological Aspects* (Eds.: P. Hänninen, H. Härmä), Springer, Berlin, Heidelberg, **2011**, pp. 1–45.
[6] D. Kovacs, E. Mathieu, S. R. Kiraev, J. A. L. Wells, E. Demeyere, A. Sipos, K. E. Borbas, *J. Am. Chem. Soc.* **2020**, *142*, 13190–13200.
[7] D. Kovacs, K. E. Borbas, *Coord. Chem. Rev.* **2018**, *364*, 1–9.
[8] S. R. Kiraev, E. Mathieu, F. Siemens, D. Kovacs, E. Demeyere, K. E. Borbas, *Molecules* **2020**, *25*, 5282.
[9] a) S. J. Butler, *Chem. Commun.* **2015**, *51*, 10879–10882; b) O. A. Blackburn, A. M. Kenwright, A. R. Jupp, J. M. Goicoechea, P. D. Beer, S. Faulkner, *Chem. Eur. J.* **2016**, *22*, 8929–8936; c) O. A. Blackburn, A. M. Kenwright, P. D. Beer, S. Faulkner, *Dalton Trans.* **2015**, *44*, 19509–19517.
[10] S.-Y. Huang, V. C. Pierre, *Chem. Commun.* **2018**, *54*, 9210–9213.
[11] a) P. R. Selvin, J. E. Hearst, *Proc. Natl. Acad. Sci. USA* **1994**, *91*, 10024–10028; b) J. Chen, P. R. Selvin, *Bioconjugate Chem.* **1999**, *10*, 311–315; c) A. M. Reynolds, B. R. Sculimbrene, B. Imperiali, *Bioconjugate Chem.* **2008**, *19*, 588–591; d) D. Kovacs, X. Lu, L. S. Mészáros, M. Ott, J. Andres, K. E. Borbas, *J. Am. Chem. Soc.* **2017**, *139*, 5756–5767; e) D. Kovacs, D. Phipps, A. Orthaber, K. E. Borbas, *Dalton Trans.* **2018**, *47*, 10702–10714; f) M. S. Tremblay, M. Halim, D. Sames, *J. Am. Chem. Soc.* **2007**, *129*, 7570–7577; g) D. Kovacs, S. R. Kiraev, D. Phipps, A. Orthaber, K. E. Borbas, *Inorg. Chem.* **2020**, *59*, 106–117.
[12] D. Kovacs, D. Kocsi, J. A. L. Wells, S. R. Kiraev, K. E. Borbas, *Dalton Trans.* **2021**, *50*, 4244–4254.
[13] D. Kocsi, D. Kovacs, J. A. L. Wells, K. E. Borbas, *Dalton Trans.* **2021**, *50*, 16670–16677.
[14] M. C. Alpoim, A. M. Urbano, C. F. G. C. Geraldes, J. A. Peters, *J. Chem. Soc. Dalton Trans.* **1992**, 463–467.
[15] L. G. Nielsen, T. J. Sørensen, *Inorg. Chem.* **2020**, *59*, 94–105.

© 2022 The Authors. Analysis & Sensing published by Wiley-VCH GmbH.

[16] D. Parker, R. S. Dickins, H. Puschmann, C. Crossland, J. A. K. Howard, *Chem. Rev.* **2002**, *102*, 1977–2010.
[17] R. Shannon, *Acta Crystallogr. Sect. A* **1976**, *32*, 751–767.
[18] T. Mani, G. Tircsó, P. Zhao, A. D. Sherry, M. Woods, *Inorg. Chem.* **2009**, *48*, 10338–10345.
[19] A. C. Harnden, D. Parker, N. J. Rogers, *Coord. Chem. Rev.* **2019**, *383*, 30–42.
[20] A. P. de Silva, H. Q. N. Gunaratne, P. L. M. Lynch, A. J. Patty, G. L. Spence, *J. Chem. Soc. Perkin Trans. 2* **1993**, 1611–1616.
[21] a) W. D. Horrocks, D. R. Sudnick, *Acc. Chem. Res.* **1981**, *14*, 384–392; b) R. M. Supkowski, W. D. Horrocks Jr., *Inorg. Chim. Acta* **2002**, *340*, 44–48; c) A. Beeby, I. M. Clarkson, R. S. Dickins, S. Faulkner, D. Parker, L. Royle, A. S. de Sousa, J. A. G. Williams, M. Woods, *J. Chem. Soc. Perkin Trans. 2* **1999**, 493–504.
[22] O. Sild, K. Haller, in *Zero-Phonon Lines And Spectral Hole Burning in Spectroscopy and Photochemistry*, Springer, Berlin, Heidelberg, **1988**.
[23] K. Suzuki, A. Kobayashi, S. Kaneko, K. Takehira, T. Yoshihara, H. Ishida, Y. Shiina, S. Oishi, S. Tobita, *Phys. Chem. Chem. Phys.* **2009**, *11*, 9850–9860.
[24] L. R. Morss, *Chem. Rev.* **1976**, *76*, 827–841.
[25] W. T. Carnall, G. L. Goodman, K. Rajnak, R. S. Rana, *J. Chem. Phys.* **1989**, *90*, 3443–3457.
[26] P. K. Glasoe, F. A. Long, *J. Phys. Chem.* **1960**, *64*, 188–190.
[27] a) K. Binnemans, *Coord. Chem. Rev.* **2015**, *295*, 1–45; b) M. H. V. Werts, R. T. F. Jukes, J. W. Verhoeven, *Phys. Chem. Chem. Phys.* **2002**, *4*, 1542–1548.
[28] P. Mandal, J. Kretzschmar, B. Drobot, *J. Biol. Inorg. Chem.* **2022**, *27*, 249–260.
[29] A. H. Harvey, J. S. Gallagher, J. M. H. L. Sengers, *J. Phys. Chem. Ref. Data* **1998**, *27*, 761–774.
[30] O. A. Blackburn, J. D. Routledge, L. B. Jennings, N. H. Rees, A. M. Kenwright, P. D. Beer, S. Faulkner, *Dalton Trans.* **2016**, *45*, 3070–3077.
[31] J. D. Routledge, X. Zhang, M. Connolly, M. Tropiano, O. A. Blackburn, A. M. Kenwright, P. D. Beer, S. Aldridge, S. Faulkner, *Angew. Chem. Int. Ed.* **2017**, *56*, 7783–7786; *Angew. Chem.* **2017**, *129*, 7891–7894.
[32] R. S. Dickins, D. Parker, J. I. Bruce, D. J. Tozer, *Dalton Trans.* **2003**, 1264–1271.

Manuscript received: March 23, 2022
Revised manuscript received: May 25, 2022
Accepted manuscript online: May 29, 2022
Version of record online: ■■, ■■■

© 2022 The Authors. Analysis & Sensing published by Wiley-VCH GmbH.

RESEARCH ARTICLE

Luminescent Eu(III) and Tb(III) complexes based on variety of macrocyclic ligands were synthesized. Addition of excess fluoride increased Eu(III) emission due to a combination of reduced O–H quenching and better Eu(III) sensitization. Cyanide addition quenched Eu(III) luminescence even when complexes with fewer inner-sphere water molecules and less O–H quenching were obtained.

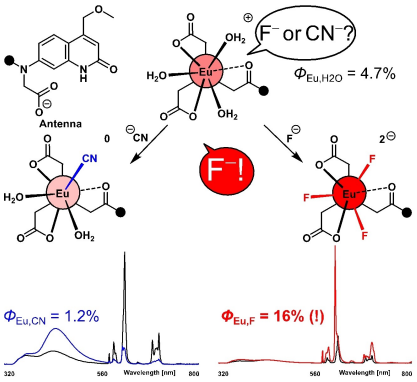

*S. R. Kiraev, R. R. Weber, Dr. J. A. L. Wells, Dr. A. Orthaber, Dr. D. Kovacs, Prof. K. E. Borbas**